Thermotherapeutic enhancement of infusate distribution during convection enhanced delivery in the brain using fiber-optic microneedle devices

Samantha Lyn Emch

Thesis submitted to the faculty of the Virginia Polytechnic Institute and State University
in partial fulfillment of the requirements for the degree of

Master of Science
In
Biomedical and Veterinary Science

John H. Rossmeisl, Chair
Theresa E. Pancotto
Shawna L. Khlan
Christopher Rylander

April 3, 2015
Blacksburg, VA

Keywords: Convection-Enhanced Delivery, Thermotherapy, Microneedle

ABSTRACT

Thermotherapeutic enhancement of infusate distribution during convection enhanced delivery in the brain using fiber-optic microneedle devices

Samantha Lyn Emch

Glioblastoma multiforme (GBM) is the most common malignant brain tumor in adults and has a median survival of 13.4 months. Convection enhanced delivery (CED) has shown promise for the treatment of GBM by allowing intratumoral delivery of therapeutics, bypassing the blood brain barrier. A fiberoptic microneedle device (FMD) CED catheter enables simultaneous delivery of laser energy and therapeutic. The laser allows for heating of tissue in the region of infusion, called thermotherapy. Thermotherapy offers the advantages of increasing the volume of distribution (V_d) of the infusate, as well as facilitating intracellular penetration of the therapeutic. *We hypothesize that heating of brain tissue will increase infusate V_d in ex vivo CED brain infusions.*

Methods: Formalin fixed mouse brains were infused by FMD-CED with Evans blue for 1 hour at 0.1 µl/min, at 22°C, 37°C and 42°C (n=4 brains/group). The V_d was determined and compared using one-way ANOVA.

Results: FMD-CED performed at 42°C resulted in significantly higher mean V_d ($4.90 \pm 2.2 mm^3$; $p = 0.03$) than those at 22°C ($1.49 \pm 0.4\ mm^3$), although no differences in V_d were observed between the other temperature groups. 42°C brains demonstrated interstitial and intracellular distribution, while rare intracellular distribution was noted in the other groups.

Discussion: The V_d of FMD-CED infusions is facilitated by sub-lethal thermotherapy. This study indicates that thermotherapeutic enhancement of infusate V_d does not occur exclusively via vascular mechanisms. Thermotherapy facilitates advective-diffusion by decreasing interstitial fluid pressure and increasing transcellular fluid transport. These results were validated in a companion *in vivo* FMD-CED study in the rodent brain.

Acknowledgements

I, Samantha Lyn Emch, DVM, am very lucky to have such wonderful people in my life to help and support me throughout this journey. I wouldn't be the person I am today without my amazing parents, who have always loved and encouraged me. I would like to thank John Rossmeisl, DVM, MS for all of his help and support. He has been a great mentor and friend in clinics as well as the lab. Thank you to the rest of my committee, Theresa Pancotto, DVM, MS, Shawna Khlan, DVM and Christopher Rylander, PhD.

Rudy Andriani, MS has been a huge help with the experimental set up, the interparenchymal pressure study and supplying the FMDs used in this study. He went above and beyond to help me and for that I will always be grateful.

Finally, I would like to thank Brett Gombar. His love and support has helped me more than words can say.

Portions of this project were funded by grants from the Wallace Coulter Foundation and National Institutes of Health (NIH/NCI 1R21CA156078). Fiberoptic microneedle device fabrication methods are described in patent applications US 13/203,800 and PCT/US2012/026,968, which are managed by the Virginia Tech Intellectual Properties Group.

Table of contents

List of Figures

List of Tables

Chapter 1: Introduction and Literature Review

1.1 Epidemiology of Brain Tumors

Intracranial neoplasia affects between 2 and 4.5% of canines in the United States [1,2]. Of these, meningiomas are the most common making up approximately 50% of primary tumors followed by glial tumors, which make up 30-40% of primary intracranial tumors. The remaining 10-20% are comprised of sarcomas, choroid plexus tumors, medulloblastomas, neuroblastomas and ependymomas. Canine necropsy studies show that 50% of intracranial tumors are secondary tumors. The incidence of intracranial neoplasms in people is similar, with about 2% of the population dying from intracranial and central nervous system (CNS) tumors [1-4]. In humans, 40% of brain tumors are of glial origin, and glioblastoma multiforme (GBM; Grade IV astrocytoma) is the most common malignant primary brain tumor in adults [5-7]. GBM follows an aggressive clinical course and carries the worst prognosis. The dog is a good model for the study of human brain tumors as both species develop these tumors spontaneously with similar incidences [8].

Dog and human primary brain tumors have similar clinical presentations and histological characteristics [8]. Some canine breeds are predisposed to the development of glial tumors such as boxers, English toy spaniels, French bulldogs, border terriers, Boston terriers, English mastiffs and English bulldogs. The median age of dogs with gliomas is 8 years [1,2,4]. In humans, Caucasians more commonly develop GBM compared to other races, and GBM appear with higher frequency in men compared to women. The majority

of people with GBM are middle aged or older with >50% diagnosed over 70 years of age [3,9].

The clinical signs are associated with the location of the tumor and the physical impact on surrounding structures. The most common clinical signs in dogs with primary brain tumors are seizures (48%), mentation changes (39%), vestibular dysfunction, circling, blindness, neck pain, anisocoria, tremors and regurgitation [1]. Oligodendrogliomas are 3.6 times more likely to cause seizures than other primary brain tumors in dogs [1]. Reported symptoms in humans are frequent headaches (50%), while 20-40% of people present with seizures as the first sign, often with a focal onset. Other common complaints include nausea, changes in cognition or personality, weakness and ataxia, urinary incontinence, aphasia, hemineglect and loss of vision [9].

1.2 Diagnosis of Brain Tumors

Due to advances in imaging techniques, antemortem diagnosis of CNS neoplasia is becoming more frequent. Magnetic resonance imaging (MRI) and computed tomography (CT) are becoming widely available in veterinary medicine and have been used for years in the diagnosis of human CNS disease. MRI is the preferred imaging modality in human and veterinary medicine. Different tumor types have variable appearances on MRI, although there is some overlap. Canine and human glial tumors have similar findings on MRI. Canine glial tumors are intra-axial, hyperintense or heterogeneously hyperintense on proton density and T2 weighted images, isointense to hypointense on T1 weighted images, have variable degrees of edema and mass effect, and have variable contrast

enhancement after intravenous administration of gadolinium. High grade tumors tend to be hypointense on T1 weighted images, have more edema, mass effect and contrast enhancement than the lower grade tumors [1,3,10,11,12]. MRI of GBM in people is characterized by heterogeneous signal on T2 weighted images, may have cystic areas, significant mass effect and peritumoral edema, indistinct tumor margins and variable contrast enhancement [3]. 64% of canine glial tumors were associated with the prosencephalon in one study [1]. The use of other forms of imaging, such as magnetic resonance angiography (MRA), proton magnetic resonance spectroscopy (H MRS) and positron emission tomography (PET), have been explored, but are much less frequently used in veterinary medicine [2].

Definitive diagnosis of brain tumors in dogs and people requires histopathological examination of tumor tissue; unfortunately cerebrospinal fluid (CSF) analysis is rarely helpful. CSF abnormalities commonly seen with glial tumors are non-specific and include elevated total protein count and mild to moderately elevated total nucleated cell count, usually mononuclear white blood cells. Rarely tumor cells are found in the CSF [2]. Histologically, glial tumors can be classified based on cell types and graded based on aggressiveness with grade I being the least aggressive and grade IV being the most [13]. It can be difficult and at times impossible to determine the cell type of origin, especially with mixed neoplastic populations. High grade (IV) astrocytomas such as GBM can occur primarily or be the result of transformation or evolution of a pre-existing low-grade glioma into a malignant form, referred to as secondary GBM [13-15]. Primary GBM is more likely to occur in elderly people and have a short clinical course whereas

secondary GBM is more common in middle-aged people with a longer progression. Histopathology is unable to differentiate between primary and secondary GBM, however there are differences in the genetic signatures of the tumors [15]. In people, 80% of high grade gliomas are GBM [7]. GBM is characterized histologically by areas of necrosis, microvascular proliferation, pseudopalisading cells, hypercellularity, anaplasia and multinucleated giant cells. In both human and canine patients, GBM is highly infiltrative, often following along the white matter and perivascular spaces, and characterized by a diffuse spread of neoplastic cells within the normal brain tissue [3,14].

As with most neoplasms, pathogenesis for development of glial tumors in dogs and people is multifactorial and not completely understood. The risk of developing glial tumors is not increased by use of cellular phones, electromagnetic fields, traumatic brain injury, aspartame or pesticides. Glial tumors are more common in specific dog breeds [1,3] and Caucasian males. The only known environmental risk factor in people is exposure to ionizing radiation. For every 100,000 people that have one CT scan performed, there will be one person who develops a glioma within 10 years [9]. Genetics also play a role with GBM development in people. Neurofibromatosis type 1 and type 2, tuberous sclerosis, familial schwannomatosis, Li-Fraumeni syndrome, Cowden syndrome and Turcot syndrome are all hereditary disease associated with an increased risk of glioma [3,9]. Human primary GBM are frequently associated with mutations in epithelial growth factor receptor (EGFR) gene, phosphatase and tensin homolog (PTEN) gene, mouse double minute 2 homolog (MDM2) gene and alterations in chromosome 10. Secondary GBM tend to contain more p53 mutations [15], and are more likely than

primary GBM to have mutations in the isocitrate dehydrogenase gene for both IDH1 and IDH2 [16]. Canine astrocytic tumors express p53 alterations less commonly with 35% of canine tumors and 60% of secondary GBM in people showing p53 changes. EGFR alterations are seen in 23% of canine astrocytic tumors vs. 40% of primary GBM in people [15,17]. IDH1 and IDH2 mutations are not seen in dog gliomas [16].

1.3 Treatment of Brain Tumors

Current treatment options for dogs with glial tumors include palliation of the clinical signs, surgical debulking, radiation therapy or a combination of the above. The mainstay of palliative treatment is corticosteroids, which facilitate stabilization of the endothelium, thereby decreasing peri-tumoral edema and inflammation. Anticonvulsants are also frequently prescribed to control seizures commonly associated with glial tumors. A recent retrospective study found the median survival time of dogs with supratentorial tumors treated palliatively was 178 days, or slightly over 25 weeks [18]. Limitations of surgical excision include disruption of the overlying anatomy, indistinct tumor borders and surgeon experience. Surgical treatment for intra-axial tumors in dogs is reported infrequently; therefore prognostic information cannot be determined [2]. Radiation therapy is the most common definitive treatment for gliomas in dogs. Median survival time for dogs with intra-axial masses treated with definitive radiation therapy was 40.4 weeks in one study [19].

In humans, the standard of care for GBMs is concurrent fractionated radiation therapy (total dose 60Gy) and temozolomide (TMZ). TMZ is an alkylating agent that is capable

of penetrating the blood-brain barrier and causes the methylation of guanine at the O6-position, which leads to apoptosis. TMZ is efficacious if the tumor does not express O6-methylguanine methyl transferase (MGMT). MGMT removes the DNA adduct caused by TMZ leading to tumor resistance. Anti-angiogenic therapy with Bevacizumab has been evaluated in GBM treatment. Bevacizumab inhibits vascular endothelial growth factor (VEGF). Concurrent treatment with radiation therapy, TMZ, and bevacizumab increased progression free survival but had no significant effect on overall survival time compared to those treated with radiation and TMZ [7,9,20]. The likely reason for the lack of benefit for overall survival time is the mechanism of action of bevacizumab. VEGF increases vascular permeability, which leads to brain edema. Inhibition of VEGF causes a significant decrease in edema and improved symptoms prolonging progression free survival but not impacting overall survival time [9,21].

Most commonly, fractionated radiation treatments are used for both dogs and people. Fractionated therapy divides the total radiation dose into several treatments, an average of 30 treatments in people [9]. Stereotactic radiosurgery may be a benefit in certain GBM relapse cases, showing a longer median survival time (20.2 months) than rescue chemotherapy protocols [22]. Radiation therapy targets cellular DNA causing either single or double strand breaks. The damage is considered lethal when double stranded breaks occur [23]. Damage occurs not only to the tumor cells, but the surrounding normal brain tissue as well. The normal tissue radiation tolerance is defined as the probability of 5% of patients developing brain necrosis within 5 years of treatment. The risk of necrosis increases as the individual fractionated dose of radiation increases [24,25]. Clinical signs

of radiation-induced necrosis mimics those of the tumor, however the clinical decline can be very rapid and severe. In one study of dogs treated with radiation, brain necrosis secondary to treatment occurred an average of 38.3 weeks after treatment and was not significantly different from survival times with tumor progression [19].

Despite aggressive treatment, the prognosis for GMB is poor. The only treatment shown to be superior to radiation as sole therapy is TMZ and concurrent radiation. The median survival time for people treated with TMZ and radiation is 13.4 months vs. 8.8 months with radiation alone. The two-year survival is 21.2% vs. 4.7% respectively [7,9]. Dogs with glial tumors also have a poor prognosis. Median survival times for dogs with brain tumors treated palliatively range from 0.8 to 25 weeks [18,26]. Treatment with radiation therapy in one study [19] reported a median survival time of 40.4 weeks for dogs with intra-axial tumors.

1.4 The Blood Brain Barrier

Glioma cells respond favorably to multiple chemotherapy drugs in vitro, however in vivo most these drugs are not efficacious when given systemically because of the blood brain barrier (BBB). The BBB is a complex interaction between multiple cell types, a basement membrane and tight junctions [27]. The endothelial cells within the brain microcirculation are different than those found in systemic circulation. Endothelial cells in the BBB lack fenestrations, have more mitochondria, decreased pinocytic activity and tight junctions between the endothelial cells. The tight junctions are formed and remain patent by a variety of proteins, specifically junctional adhesion molecules (JAM-1, -2, -

3), occludin and claudins (-1, -3 and -5) [27,28]. The JAM family has an important role in development of the tight junctions as well as regulation of BBB leukocyte permeability. Occludin molecules are responsible for maintaining resistance to charged molecules within the tight junctions. The claudins seem to have a role in the initial formation of the tight junctions and, in combination with occludin, help to maintain its integrity [27,28].

Pericytes are found outside of the endothelial cells in the BBB and surrounded by a basement membrane, the basil lamina. The role of pericytes in the BBB is not well understood, but thought to be related to management of blood flow. Contractile proteins have been found within these cells allowing regulation of the size of the capillaries. Periocytes secrete angiopoetin, inducing the production of occludin, suggesting that they also play a role in maintenance of the tight junctions between endothelial cells [27]. The basil lamina surrounding the endothelial cells and pericytes is 30-40nm thick and is composed of type IV collagen, heparin sulfate proteoglycans, laminin and fibronectin along with other matrix proteins [27,28]. The final anatomic component of the BBB is astrocytes. Astrocytes have foot process, which surround about 90% the capillaries; the basil lamina is contiguous with the plasma membrane of these foot processes. Astrocytes have a large and diverse role in the BBB. They are thought to play a role in the development and maintenance of the BBB as well as help manage the microvascular permeability in real-time along with neurons [27,28].

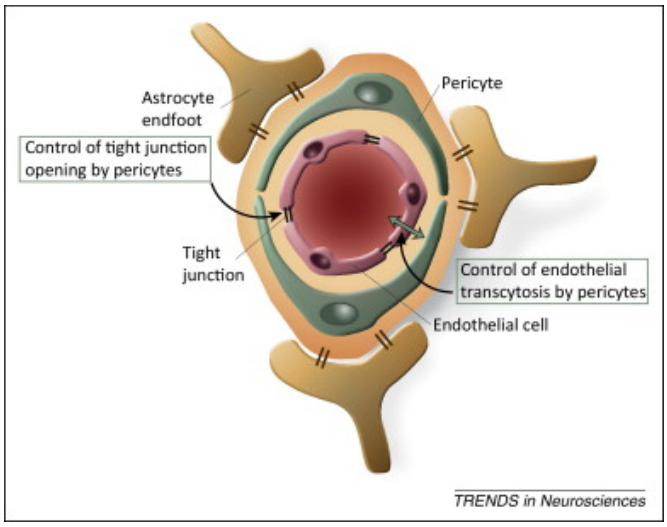

Figure 1 – Illustration of the blood brain barrier and the cellular interactions. Image taken from an open access source [31]. https://s100.copyright.com/AppDispatchServlet?publisherName=ELS&contentID=S0166223614000599&orderBeanReset=true, used under fair use, 2015.

The complex anatomy of the BBB results in the prevention of large molecules (>400Da) from entering the parenchyma of the central nervous system. The barrier is also hydrophobic and has a high electrical resistance, therefore preventing the movement of charged or polar molecules and water-soluble molecules through it [28,29]. Because of these properties, most toxins and drugs cannot gain entrance into the brain. Another obstacle facing pharmaceuticals are specific efflux pumps located within the BBB. The most extensively studied is P-glycoprotein, which is in the multidrug resistance (MDR) gene family. P-glycoprotein is found on the luminal membrane of the endothelial cells and will actively pump molecules that diffuse across the endothelial membrane back into circulation. Other drug efflux pumps include the multidrug resistance (MRP) family

(MRP1-9 have been found within the BBB) and the breast cancer-resistant protein (ABCG2 gene). Organic anion and cation transporters (OAT-1 and -2) are also found in the BBB, however they rely on passive transport across concentration gradients and can move molecules into or out of the brain depending on the gradients [27-30].

Several different methods have been studied to cause temporary disruption in the BBB to allow for drug delivery to the brain. Injection of osmotic agents, such as mannitol or arabinose, into the carotid artery causes the endothelial cells to shrink and the tight junctions open for a few hours, allowing passage of drugs. Osmotic opening is indiscriminate, however, leading to neurologic side effects after cytotoxic drugs come in contact with normal brain tissue [28,29]. Chemical opening involves the administration of a drug causing disruption in the BBB. Bradykinin has been shown to increase BBB permeability within tumor capillaries without effecting normal brain capillaries. Clinical trials using bradykinin or its analogs reported severe tachyphylaxis, systemic toxicity, and a very short time window of BBB disruption [28]. Focused ultrasound can also transiently increase BBB permeability without causing neuronal damage, and in vivo rodent studies are promising [32]. Molecules that inhibit drug efflux transporters have also been studied; however, often result in severe systemic and neurologic toxicities. Radiation therapy can disrupt the BBB by causing vessel dilation, thickening of the vessel walls, altering the endothelial nuclei, inducing astrocyte hypertrophy and decreasing P-glycoprotein expression. Stabilizers and solvents (sodium doecylsulfate, ethanol dimethylsulfoxide, glycerol, etc) often used in the development of vaccinations or therapeutics also can disrupt the BBB. Regardless of how it is accomplished, disruption

of the BBB results in astrocyte toxicity secondary to exposure of plasma proteins to the brain, astrogliosis, vascular pathology and other neuropathologic changes within the brain [28-30].

On the other hand, some researchers have been looking at ways to alter pharmaceuticals to get through the BBB. The lipidization of small molecules involves the conversion of water-soluble drugs into lipid-soluble drugs that could pass through the BBB. This is difficult to do, while maintaining small (<400Da) molecules. The best example of this is heroin, which is the acetylation of morphine to make it lipid-soluble. Heroin readily crosses the blood brain barrier, once within the brain it is transformed back to morphine and cannot leave the brain causing prolonged activity [30]. A theory that may be better than lipidization, is the utilization of available transporters to move the therapeutic into the brain. Two examples are carrier-mediated transport, such as glucose transporters (GLUT-1) and receptor-mediated transport, such as insulin receptors (INSR). By combining the drug with a substrate for a carrier or receptor already present, the drug will be transported through the BBB. A similar method of transport, called molecular Trojan horse, involves monoclonal antibodies attached to the therapeutic of choice. The antibody then binds to a transporter and the drug follows the antibody through the BBB. Most of these methods do not specifically target diseased areas in the brain and there is the potential for neurotoxicity as with the methods that disrupt the BBB [29,30].

As one would assume from the fact that many brain tumors are contrast enhancing on neuroimaging, the BBB is not normal within the tumor. This has been studied in both

primary brain tumors and metastatic brain tumors. Changes to the BBB include alterations in the endothelial tight junctions, increased perivascular spaces, the presence of endothelial fenestrations as seen in the periphery and an increase in pinocytosis. With metastatic tumors, the endothelium resembles that of the tissue of origin rather than the brain [28,32]. There is often altered expression of drug transports, specifically P-glycoprotein. In malignant gliomas, there is conflicting evidence in regards to altered P-glycoprotein expression. This all results in increased permeability in brain tumors, however this permeability is very heterogenous and there are often tumor cells that extend beyond the areas of BBB permeability preventing systemic chemotherapy from causing a significant effect. That being said, chemotherapeutics given systemically are often found at a higher concentration within the tumor tissue than the surrounding normal brain tissue. Metastatic tumors often respond to systemic chemotherapy the same as the primary tumor or non-CNS metastatic disease [28,32].

1.5 Convection-Enhanced Delivery

One way to bypass the blood brain barrier is to deliver therapeutics directly to the brain tissue. This can be done by diffusion and convection-enhanced delivery. Carmustine wafers are often implanted within the tumor resection cavity in human GBM patients. The carmustine relies on diffusion to kill glioma cells that remain after surgery. This is the only locally delivered chemotherapy technique, which has been shown to provide benefit in a limited number of patients. The problem with diffusion is the extremely high concentration gradient of the drug required to generate adequate distribution in the peritumoral tissue can cause toxicity to surrounding brain tissue. Diffusion from the

carmustine wafers causes effective concentrations of the drug within only a few millimeters into the brain, where as 80% GBM recur within 2cm of original mass [33,34].

An alternative to diffusion is a process called Convection-enhanced delivery (CED). This procedure allows for infusing the brain directly with therapeutic drugs without relying on diffusion. This treatment modality is being researched for treatment of brain neoplasms, neurodegenerative diseases, epilepsy and stroke [35]. CED overcomes the need for diffusion by providing a positive and continuous pressure gradient. The therapeutic is distributed within the extracellular spaces by taking advantage of the naturally occurring hydrostatic and oncotic pressure gradients within the brain [36,34]. White matter is highly conductive and grey matter has a lower conductivity, which accounts for vasogenic edema occurring throughout white matter [36]. Vasogenic brain edema and infusate distribution both occur through bulk fluid flow and to a lesser extent diffusion [34]. Darcy's flux (equation shown below) shows that infusate flow through tissue is directly related to the difference between the infusion and tissue pressures and inversely related to the resistance of the tissue [35].

$$\text{Flow} = \Delta\text{Pressure} / \text{Resistance}_{\text{tissue}}$$

CED can distribute a significant amount of drug without causing significant increase in intracranial pressure or tissue volume [34]. CED is performed by placing an indwelling catheter(s) directly into the brain or tumor tissue, then infusing the therapeutic at a constant rate. CED has been successfully performed on rodent models, canine models, primate models, canine glioma patients and humans using various chemotherapeutics and

carriers. The most common complications encountered in CED studies include leakage of infusate into a ventricle or the subarachnoid space and backflow along the catheter tract [37-40]. CED has many advantages over systemic administration of chemotherapy drugs for treating brain neoplasia, however many phase III clinical trials have failed demonstrate a clinical advantage. Possible causes for the less than expected outcomes include poor catheter placement, too low concentration of infusate, flow rate either too slow or too fast, and back flow along the catheter track with leakage into the subarachnoid space. These complications can all lead to inadequate drug delivery to the affected tissues [33,39].

Back flow, also termed reflux, along the catheter track is a significant complication and can prevent distribution of the infusate to the desired tissue. This back flow can happen secondarily to mechanical disruption of the tissue during catheter placement, which allows for a void to form around the outer wall of the catheter. Another reason for reflux is the intrinsic backflow pressure associated with the infusion process. The infusate pushes against the tissues, causing them to separate from the catheter [36]. Backflow is directly related to the viscosity of the substance infused, flow rate, catheter diameter and the location of the cannula tip. Small diameter catheters, soft catheters, fluid outlet located away from the tip of the catheter, step down catheters and polymer coatings have all been shown to decrease the amount of reflux [36,41].

Within tumors, the interstitial fluid pressure (IFP) is often heterogeneously elevated making it more difficult to evenly distribute therapeutics via CED over the intended area

and often the drug concentrations within the tumor are variable [36]. Cystic regions within tumors may have a lower pressure causing the infusate to accumulate within these areas of lower pressure, as with leakage into ventricles or the subarachnoid space, preventing adequate infusate distribution. Elevated IFP in tumors is thought to partially occur due to changes in the local microvasculature. Hyperthermia damages the microvasculature lowering the IFP of tumors [42]. Infusate distribution, as mentioned earlier, occurs through the interstitial space, however also by passive and active transport across cell membranes and via blood perfusion. All of these pathways are temperature dependent [43,44].

1.6 Thermotherapy

Not only can hyperthermia help with conduction of therapeutics, it can potentate the activity of some chemotherapeutic medications by allowing the drug to permeate the cell membrane more readily. Lower temperatures cause the cell membrane lipids to be tightly packed together, whereas higher temperatures cause the opposite easing the drug entrance into the cell. Elevated temperatures can also increase cellular metabolism and inhibit enzymes making the cell more susceptible to chemotherapeutics [43,45]. It would be advantageous to have immediate intracellular movement of a therapeutic when delivered via CED because it would limit the amount of drug metabolized after delivery before reaching the target and drug loss through tumor capillaries. It has also been shown that areas of elevated IFP have increased rates of infusate efflux after CED [36]. Performing CED with concurrent hyperthermia may allow for a larger infusate volume of distribution throughout the tumor and peri-tumoral tissues by increasing fluid advective diffusion

(convection), intracellular transport (both passive and active), blood perfusion as well as decreasing the infusate viscosity [43].

Therapeutic hyperthermia has been used for the treatment of many types of cancers via whole body hyperthermia, regional hyperthermia or local hyperthermia. Many different methods of inducing hyperthermia have been documented including radiofrequency, ultrasound, laser and microwave/electromagnetic field hyperthermia [46-49]. These techniques have been used alone or in conjunction with chemotherapeutics to induce either lethal or non-lethal hyperthermia. Thermal damage to cells depends on the degree and the duration of hyperthermia. Cellular changes include increased membrane permeability, denaturation of membrane and cytoskeletal proteins, membrane blebbing, collapse of the cytoskeletal proteins and cell lysis [44,50]. Temperatures between 43°C and 45°C can cause reversible changes to the cell membrane and enzymatic activity, however if these temperatures are sustained for >25 minutes, the effects are permanent and lethal. Neoplastic cells may be more sensitive to lethal injury at these temperatures than normal cells [51]. Temperatures >45°C will cause irreversible tissue coagulation [50,51]. Lethal hyperthermia can be problematic within the brain; leading brain, necrosis, edema and the potential for elevated intracranial pressure and neurological decline.

In conjunction with the laboratory of Dr. Christopher Rylander, we have been developing fiberoptic microneedle catheter devices (FMD) specifically for local brain infusions. The FMD have been shown to be able to simultaneously infuse soluble agents and deliver uniform and diffuse optical energy along their length [52]. The delivery of 1064nm laser

light via the FMD catheters has been tested in vitro and in vivo [43,53]. This wavelength was chosen because it has lower scattering coefficients than lower wavelengths, along with lower absorption coefficients for various types of brain tissue. This allows the light to penetrate deeper into brain tissue [54]. A recently published study by Hood et al. in 2013 [55], using this device showed laser power of 100mW did not cause any thermal damage to brain tissue in rodent models. This same study showed that a power of 200mW caused lethal thermal injury confined to a small area around the tip of the FMD and powers >200mW caused severe and lethal cellular changes more diffusely. Previous studies have shown that a power of 100mW to cause hyperthermia with a mean temperature of 38.7°C and 200mW to cause a mean temperature of 42°C [55]. The FMD has several advantages over traditional CED catheters including a small inner diameter of 450μm, step down design, and the ability to simultaneously deliver infusate and laser energy. The ability to deliver infusate while inducing local hyperthermia prevents additional mechanical damage to overlying brain tissue if multiple devices were inserted. It also allows for heating of the infusate, decreasing its viscosity and preventing it from cooling the tissue if infused at room temperature; both of which can improve tissue delivery. For larger animal models or tumors, there is an arborizer that can be used with up to 7 FMDs at the same time. The arborizer allows for a single 12G catheter to be inserted into the brain with the individual FMD exiting the arborizer at 30° angles. This allows for multiple points for treatment at the same time [56].

Given the poor prognosis with glial tumors, even with aggressive therapy, new treatment modalities need to be developed and improved. CED has great promise for the treatment

of these tumors despite the fact that clinical trials have failed to show any benefit as of yet. By improving therapeutic delivery to the tumor tissue, improved tumor control may be achieved. The goal of this project is to further elucidate the potential mechanisms by which hyperthermia increases the volume of distribution during local intraparenchymal infusions in the brain. The experiments described here are complimentary to in vivo studies specifically investigating the effects of local hyperthermia delivered via FMD devices on the volume of infusate distributions in the brain. ***We hypothesize that thermotherapy will increase the volume of distribution of infusates delivered locally to the brain using CED compared to CED infusions performed at basal temperatures.***

Chapter 2: Method and Materials

2.1 Ex vivo Mouse Brains and Infusion Preparation

The brains of fifteen adult male, Balb-c mice were used for this study. The mice were previously humanely sacrificed according to procedures approved by the Virginia Tech Animal Care and Use Committee (protocol #11-019-SBES) and the brains fixation-perfused through cannulation of the carotid artery immediately prior to sacrifice. The brains were removed en bloc from the olfactory bulb to the cervicomedullary junction from all the mice and stored in 10% neutral buffered formalin until ready for use.

The brains were removed from the formalin and immobilized by embedding them ventrally and laterally in 0.6% wt agarose gel (Sigma-Aldrich, St. Louis, MO) within a cell culture plate (TC-6W, EMD Millipore, Billerica, MA) leaving the dorsal surface of the brain free of agarose. The agarose was made according to the manufacturers instructions. The cell culture plates were then placed in a circulating water bath (Thermo Scientific Precision, Fisher, Waltham MA) to maintain the desired temperature throughout the procedure, and stabilized with a weight. A thermocouple (K-type, Omega Engineering, Stamford, CT) was used to monitor the temperature of the water bath as well as the temperature within the brain tissue throughout the procedure.

2.2 Fabrication and Specifications of the Fiberoptic Microneedle Device (FMD)

The FMD were manufactured according to previously described methods [53]. Briefly, the FMD is composed of a hollow fiberoptic (HF) capable of delivering both fluids and

light simultaneously. The HF is commercially available, light-guiding, fused silica capillary tubing (365 μm outer diameter, 150 μm inner diameter, Polymicro Technologies, Phoenix, AZ) angle-polished at the tip to produce a sharp, beveled microneedle, as demonstrated in Figure 2. The HF is manufactured with a 40-60 μm polyimide jacket around the outer cladding layer to provide lateral support and protection. To fabricate a prototype capable of co-delivery, the HF was coupled with both a solid, multi-mode fiberoptic (SF, 80 μm outer diameter, 50 μm core diameter, Polymicro Technologies, Phoenix, AZ) and a 30G syringe needle (Becton, Dickinson, Franklin Lakes, NJ) sheathed inside 450μm inner diameter fused silica capillary tubing (TSP450670, Polymicro Technologies, Phoenix, AZ). To ensure high light coupling efficiency, the SF was fusion spliced to the annular core of the HF with subsequent manual alignment of the fiberoptics [53]. Once spliced, the aligned joined fibers were placed within a protective length of TSP450670 fused silica capillary tubing (inner diameter 450 μm, Polymicro Technologies, Phoenix, AZ). A 30G syringe needle was inserted parallel to the SF and placed in close proximity to the splice inside the sheath, enabling fluid coupling to the HF through the Luer-Lok connector as shown in Figure 2. The non-spliced end of the HF was polished at an approximately 45º angle to create a sharp, microneedle profile to ease insertion into brain tissue (Figure 2).

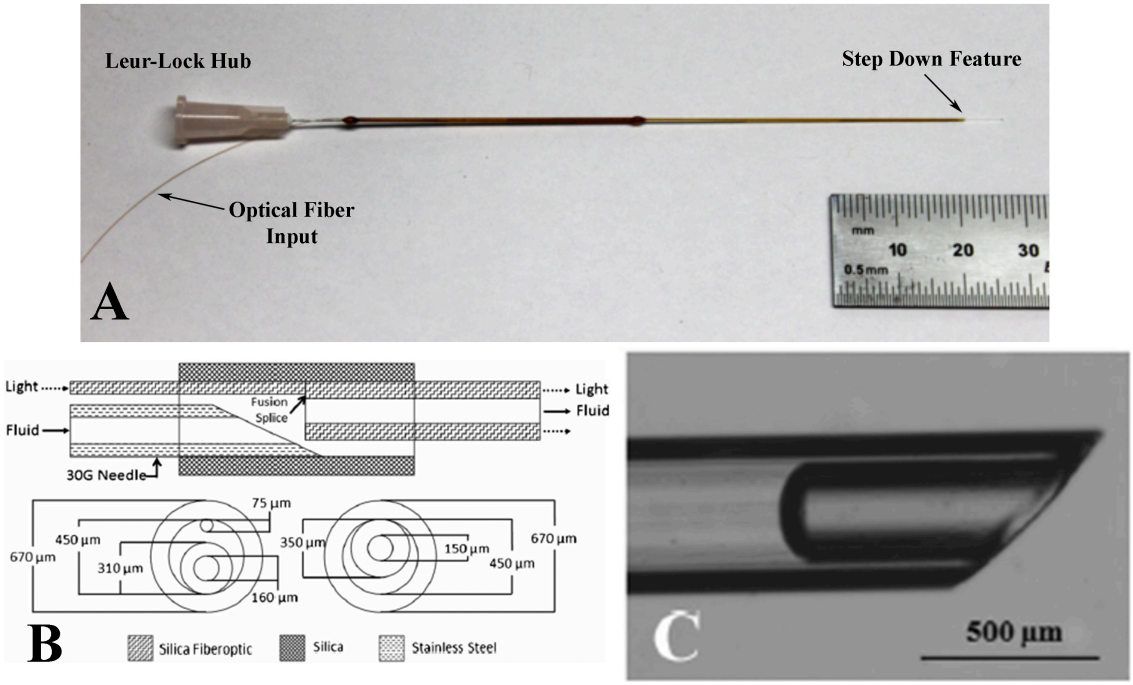

Figure 2- A- Fiberoptic microneedle device (FMD) used for convection enhanced delivery in this study capable of simultaneous co-delivery of light and fluids, and featuring a reflux preventing step down feature at the distal tip of the device. (A) capillary tubing outer sheath surrounds the FMD for additional support. (B) Schematic of FMD co-delivery couple design. (C) Polished and sharply beveled FMD tip. Figure modified from Hood RL, Rossmeisl Jr JH, Andriani RT, et al. Intracranial hyperthermia through local photothermal heating with a fiberoptic microneedle device. Lasers Surg Med 2013; 45(3):167-174.

2.3 CED Infusion Procedure

A stereotactic head frame outfitted with a manipulator arm (Model 1530M, Kopf Instruments, Tujunga, CA) was positioned such that that the rostrocaudal bars were oriented parallel to the long axes of the rectangular basin of the water bath and

rectangular cell culture plate (Figure 3). A single FMD catheter was mounted to the needle holder of the manipulator arm of the frame, which was subsequently used to precisely guide placement of the FMD in to the left cerebral hemisphere of each mouse brain at the following stereotactic location, referenced to the bregma and dorsal midline: bregma zero (z = 0 mm), left lateral (x = + 3 mm), dorsoventral (y = - 2 mm), as defined by Paxinos and Franklin [57], which accounts for 25% linear shrinkage of the brain during fixation (Figure 4). A thermocouple probe, which was also affixed to the manipulator arm in a parallel position to the FMD was placed in the homologous location in the contralateral (right) cerebral hemisphere of each mouse brain.

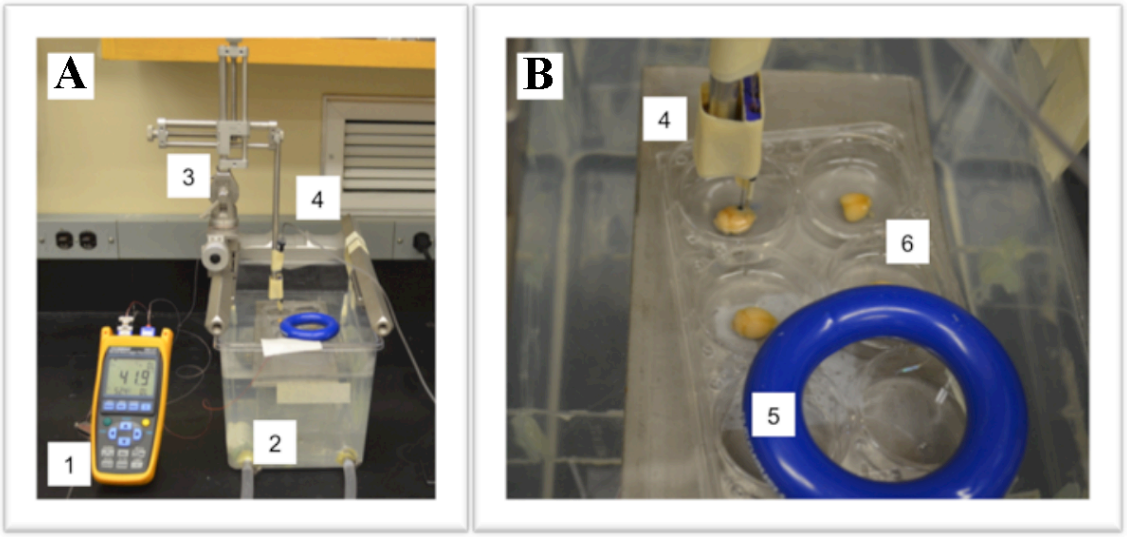

Figure 3- Experimental setup for CED infusion (A) with a zoomed in image showing the FMD and temperature probe inserted into a brain (B). 1 – thermocouple; 2 – water bath; 3 – stereotactic head frame; 4 – manipulator arm with FMD and temperature probe attached; 5 – weight; 6 – cell culture plate with agarose embedded brains.

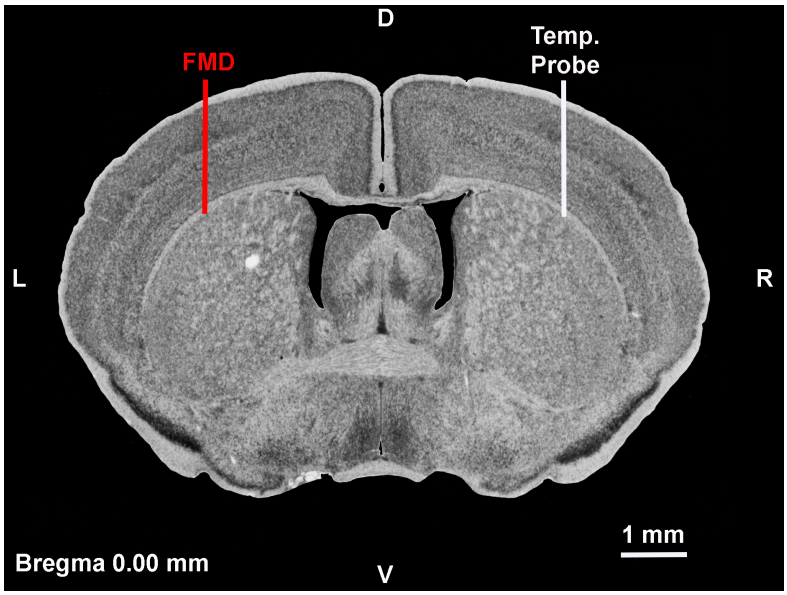

Figure 4- Nissl stained, 5 µm thick transverse section of adult mouse brain obtained at the level of the bregma. The stereotactic coordinates used for insertions of the FMD (red) and temperature probe (white) are schematically presented. Photo courtesy of the Veterinary and Comparative Neurooncology Lab, Virginia Tech.

A solution of Evans blue dye (2.5%, Sigma, St. Louis, MO) was infused through the FMD into the left cerebral hemisphere at a rate of 0.1µl/min for one hour (total volume infused [V_i] = 6 µl) using a syringe pump (Ph.D Ultra, Harvard Apparatus, Holliston, MA). Brains were infused at room temperature (22°C, n=4), body temperature (37°C, n=4) and an elevated temperature (42°C, n=4). This elevated temperature was chosen, because it has been shown that temperatures ≥42°C cause thermal damage to cells, although the damage at 42°C is minimal [55]. It has also been shown that temperatures between 39°C and 41°C increase chemotherapy induced cytotoxicity, without a significantly increased benefit at higher temperatures [58]. The temperature of the water bath and the brain were recorded every 5 minutes throughout each infusion.

2.4 Intraparenchymal Pressure (IPP) of Formalin Fixed Mouse Brains

A pilot experiment was performed in which the intraparenchymal pressure (IPP) of the brain was measured in both hemispheres of 3/15 agarose embedded mouse brains using a parenchymal pressure catheter (SPR-320, Millar Instruments, Houston, TX) with 660 μm tip diameter connected to a controller unit (TC-510, Millar Instruments). The pressure catheter tip was inserted into the brain using the same stereotactic coordinates, as described above, that were used for the infusions. The IPP was recorded at 50 Hz using a TC-100 recording system (Biopac, Santa Barbara, CA) and allowed to equilibrate for 10 minutes after catheter insertion. Intraparenchymal pressure values were then recorded every 2 minutes for ten minutes and the results averaged. Bilateral hemispheric IPP measurements were made for one brain each at 22°C, 37°C, and 42°C. The three brains in which IPP measures were obtained were not subjected to CED infusion procedures.

2.5 Calculation of the Infusate Volume of Distribution (V_d)

Immediately after the infusions, the brains were removed from the agarose and serially sectioned in a 1 mm rodent brain matrix slicer (Zivic Instruments, Pittsburg, PA). The sections with visible Evan's blue were digitally photographed (Canon DS126071, Melville, NY) with an embedded metric scale bar. If the Evan's blue was grossly different on the rostral vs. caudal side of the 1mm section, a photograph of each side was taken, if there was no gross difference between the sides, a photograph of just the caudal side was taken. The photographs were uploaded into a commercially available computer

program (NIS Elements AR, Nikon, Japan). Through this program, a manually defined region of interest (ROI) outlining the grossly visible Evan's blue infusion was determined from each slice, and the area calculated from the ROI of each slice using the area function of the software. This step was repeated 3 times for each section and the mean area was used to calculate the total volume of distribution (V_d) for each brain. The cavalieri principle was used to calculate the V_d using the following equation [59].

$$V_d = A \times d$$

Where A is the measured area and d is the distance between the area measurements, or in this case, slice thickness (1mm). If the grossly visible Evan's blue was different between the rostral and caudal sides of the section, the area was determined for each side and the slice thickness was halved to 0.5mm when calculating the volume. The volume for each slice was then added together to determine the total brain V_d.

2.6 Histomorphological Evaluation of CED Infusions

Individual transverse brain sections were embedded in paraffin, sectioned at 5μm intervals using a microtome, counterstained with hematoxylin (Sigma, St. Louis, MO) and examined by light microscopy (Nikon Eclipse Ni-E, Nikon, Japan) for qualitative distribution characteristics of the Evan's Blue infusate in the cerebral cortex.

2.7 Statistical Analysis

The statistical analysis was completed using commercially available software (SAS version 9.4, SAS Institute, Cary, NC). One-way ANOVA was performed to compare the IPP between both hemispheres of the pilot experiment and the IPP between each of the

temperature groups. One-way ANOVA was also performed to compare the V_d between the three temperature groups. A mixed-model ANOVA was performed to determine if there was significant variation between the brain temperature and the goal temperature in each of the 3 groups. The coefficient of variation was calculated to determine if there was a significant variation in temperature throughout each infusion.

Chapter 3: Results

3.1 CED Infusion Procedure

In total, 11/12 CED ex vivo infusions were completed without procedural complications. Significant reflux along the FMD insertion track and brain surface was observed in one of the brains assigned to the 37°C group, which prevented accurate measurement of the V_d, and thus exclusion from data analysis (Figure 5).

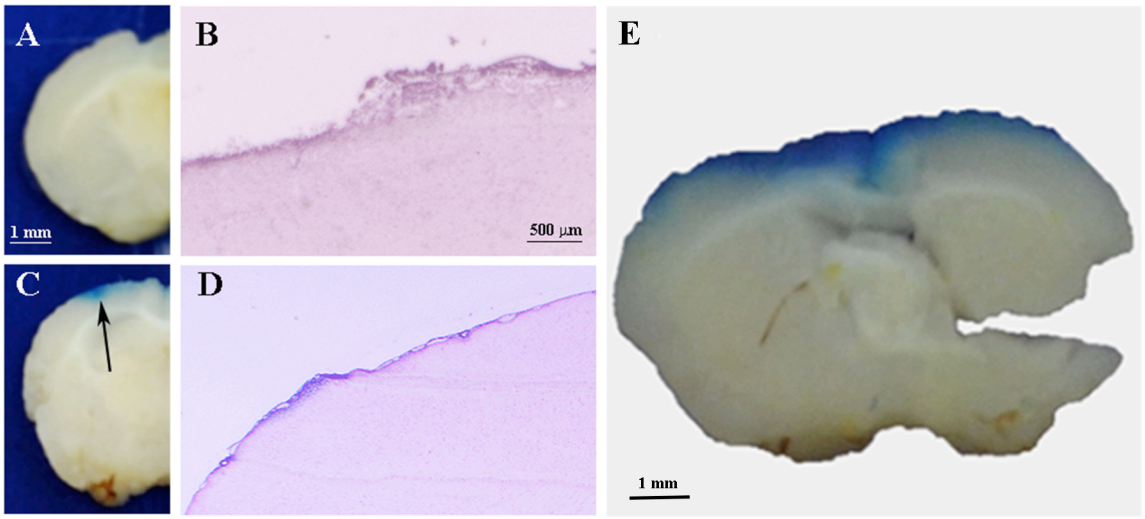

Figure 5- Examples of unacceptable reflux of Evan's Blue infusate onto the brain surface during CED infusion. Gross photograph (A) and photomicrograph (B) of an untreated, normal brain. Gross photograph (C) and photomicrograph (D) of surface reflux (arrow). E- Massive reflux along the dorsal surface of the brain eliminated one infusion from analysis in the 37°C group.

3.2 Intraparenchymal Pressure (IPP) of Formalin Fixed Mouse Brains

Brain temperature had a significant and negative association with IPP (Table 1). There were no significant differences between IPP measurements between the right and left cerebral hemispheres of each brain.

	Mean IPP (mmHg)		
Temperature	22°C[a]	37°C[b]	42°C[c]
Left cerebrum	$8.4 \pm 2.3^{b,c}$	$4.9 \pm 2.1^{a,c}$	$2.4 \pm 1.3^{a,b}$
Right cerebrum	$8.7 \pm 1.8^{b,c}$	$4.7 \pm 2.0^{a,c}$	$2.6 \pm 1.5^{a,b}$

Table 1- IPP measurements for each of the 3 temperature groups. Superscripts denote group means that are significantly different ($p < 0.05$).

3.3 Calculation of the Infusate Volume of Distribution (V_d)

The Mean V_d for the 22°C group is 1.46mm^3, the 37°C group is 3.47mm^3 and 5.13mm^3 for the 42°C group, see table 2. There was a significant difference in V_d between the 22°C group and the 42°C group ($p = 0.03$). The difference was not significant between the 22°C and 37°C groups ($p = 0.32$) or the 37°C and 42°C groups ($p = 0.44$), although for both of these comparisons, the V_d was larger in the group with the higher temperature, see table 2 and figures 6 and 7.

Temperature Group	Sample Size	Mean mm^3	SD	Minimum mm^3	Maximum mm^3	Vd/Vi
22°C	4	1.46	0.42	1.05	1.83	0.24
37°C	3	3.47	1.89	2.07	5.62	0.58
42°C	4	5.13	2.24	2.66	8.08	0.86

Table 2- Volume of distribution metrics by temperature

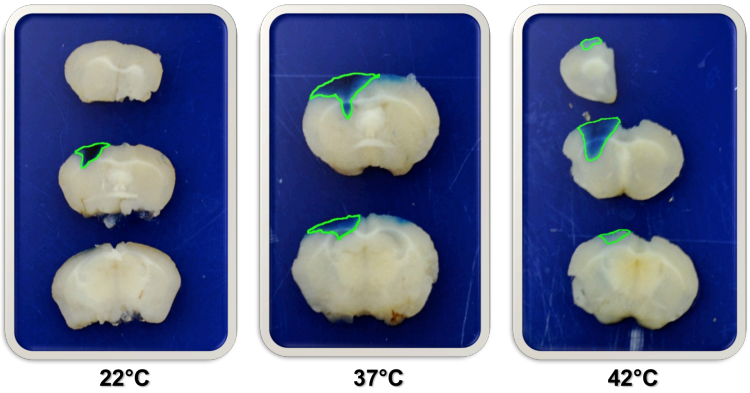

Figure 6- Representative gross brain CED infusion results for different groups. The green outline represents the ROI used to calculate the area of the infusion.

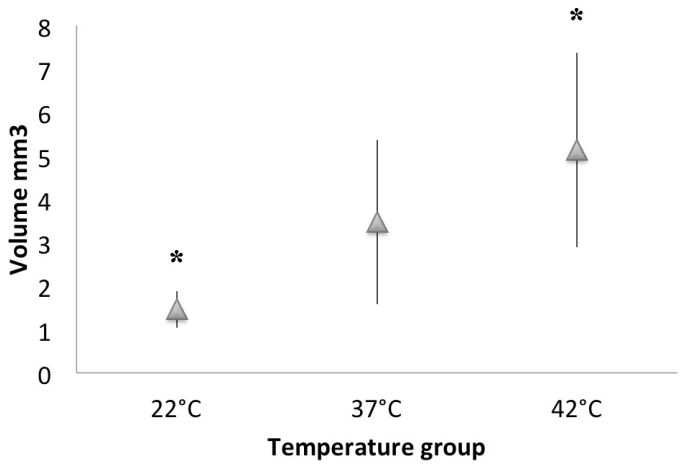

Figure 7- Quantitative comparison of V_d of CED infusions. The bars indicate the standard deviation from the mean, which is represented by the grey triangles for each of the temperature groups. The asterisks (*) indicates statistical significance.

A significant difference was found between the target brain temperature and measured brain temperature in the 22°C group (P=0.0004). The mean actual temperatures for the four brains in the 22°C group are 24.4°C, 23.3°C, 22.6°C and 23.0°C. There was no significant difference between the actual temperature and goal temperature for the 37°C and 42°C groups. The coefficient of variation is <5 for all groups, indicating that the variation between temperature for each infusion is negligible, see table 3.

Temperature group	Mean CV
22°C	2.05
37°C	1.40
42°C	0.91

Table 3- Mean Coefficient of variation for infusions in each of the 3 groups.

3.4 Histomorphological Evaluation of CED Infusions

Sections of cerebral cortex, hippocampus and white matter were prepared and counter stained with hematoxylin for each of the 3 temperature groups and untreated sections, for comparison. The untreated sections were taken from the contralateral hemisphere. The stained sections (see figure 8 below) of brains in the 42°C group, showed observably more intracellular Evan's blue than the other two groups in all 3 anatomic locations. The 37°C sections had slightly more intracellular Evan's blue than the 22°C sections which had minimal intracellular dye. The interstitial Evan's blue was subjectively darker in the 42°C sections compared to the other two groups and subjectively darker in the 37°C sections compared to the 22°C sections. The 22°C cortex slide showed a large amount of vacuolization compared to the other temperature groups and the untreated section. This vacuolization was also present in the 22°C hippocampal section, but to a lesser degree. There was no evidence of thermal cell damage in all three temperature groups.

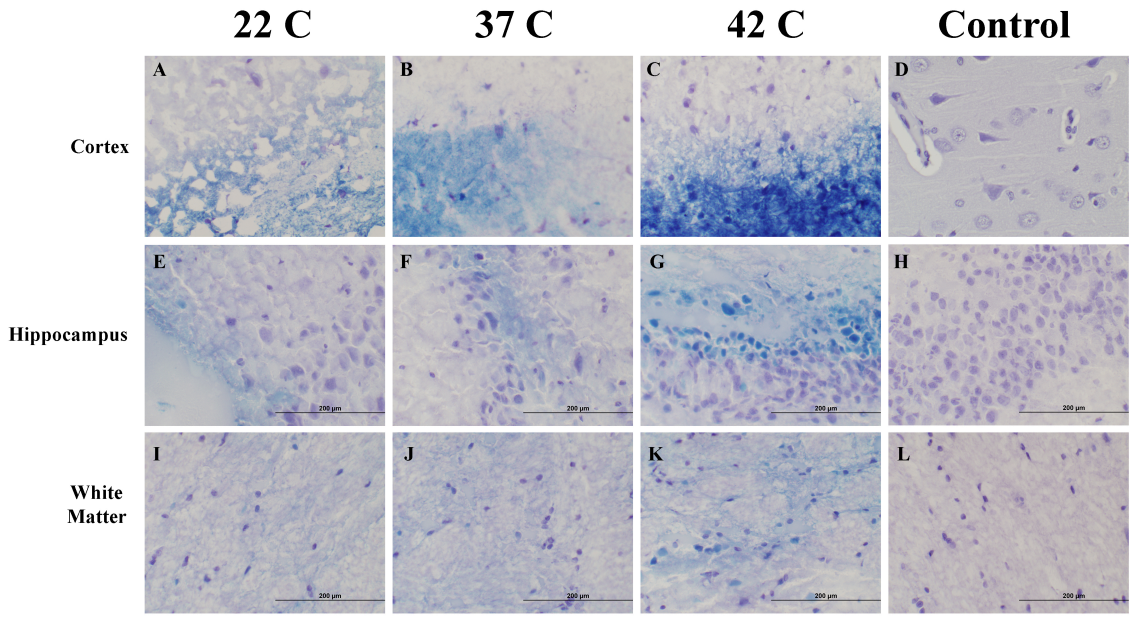

Figure 8- Hematoxylin counterstained histomorphology of CED infusions and untreated controls (40X magnification). Note the large amount of intracellular Evan's blue in the 42°C slides (C, G and K) compared to the other two temperature groups. There is also more diffuse interstitial Evan's blue in the 42°C slides. There is minimal intracellular Evan's blue in the 22°C slides (A, E and I). Note the slight peri-cellular clearing in slide D, which is an artifact, compared to slide A with significant peri-cellular vacuolization.

Chapter 4: Discussion

There was a significant difference in the V_d between the 22°C group and the 42°C group which was expected. There was not a significant difference between the 22 °C and 37°C groups and 37°C and 42 °C groups, which was not expected. The most likely cause for this is the small sample size, especially since one brain was excluded in the 37°C group due to reflux along the catheter track. Reflux is one of the most common complications with CED, resulting in treatment failure. The in vivo rat study [43] using the same FMD catheter had an incidence of reflux of 1 out of 30 infusions (3.3%) compared to 1 out of 12 brains (8.3%) in this study. Previous rodent studies have shown reflux of <30% with flow rates ≤5.0µl/min, higher flow rates lead to more frequent reflux [34]. The frequency of reflux is dependent on many factors, such as; catheter diameter, infusion rate, infusate viscosity and anatomic catheter placement, therefore direct comparison of reflux frequency to rodent studies not using FMD is not possible.

The infusion rate of 0.1µl/min was chosen because it is the same rate used in the rat study [43]. Previous rodent studies have shown infusion rates between 0.5 and 5µl/min in small animal models to be effective where as higher rates, over 6.2µl/min, cause more reflux and leakage into the subarachnoid space [34]. Evans blue was used in this study because of its availability, price and to remain consistent with the in vivo rodent study [43], which used Evans blue for half of the infusions. Evan's blue is also very easy to visualize grossly within the tissue after the infusions. Properties of the infusate itself, such as the viscosity and charge may alter the V_d. The main goal of this study was to determine if the V_d was positively correlated with increasing temperature, not to mimic

the infusate characteristics of therapeutics. Therefore, we did not feel the need to use a potentially cytotoxic substance as would be used in vivo to treat tumors.

The purpose of this study was to determine if the elevated tissue temperature was responsible for the increased V_d found in the in vivo rodent study with the same FMD catheters [43], and try to elucidate mechanisms of volumetric distribution. The volumes in this study are not translatable to the V_d expected for in vivo infusions. The V_d is going to be dependent on characteristics of the tissue and the infusate. The brains infused in this study were fixed in formalin, which alters the tissue properties. Formalin fixation results in the binding of aldehyde groups to proteins leading to methylene bridges (crosslinking between the bound proteins). Other molecules become trapped in the crosslinks stabilizing the tissue [60]. Undoubtedly fixation changes the properties of the tissue and the V_d would not be the same as in vivo brain or tumor tissue. This is likely the main reason the V_d/V_i ratios were so small in this study. The in vivo rat study [43] had considerably larger V_d/V_i ratios. Control brains, which had the infusion through the FMD at body temperature, had a mean V_d/V_i ratio of 1.70, brains treated with 100mW laser (38.7°C) had a mean ratio of 2.63 and brains treated with 200mW laser (42°C) had a mean ratio of 3.00.

The IFP of normal tissue is close to zero. The IFP within brain tumors varies based on the size of the tumor and systemic treatments received (corticosteroids or diuretics). Reports of IPP in human brain tumors varies from 8-0.7 mmHg after receiving systemic treatments to decrease the pressure. CSF pressure in humans with brain tumors prior to

any systemic treatment has been measured at 24-33mmHg with the CSF pressure being similar to the IFP in both health and disease. Rodent studies have found IFP within brain tumors, without systemic treatment, to be 9-25mmHg [61]. The IPP found in this study was higher than that expected for normal brains, which is likely because the tissue was formalin fixed, making fixed brain tissue a good model for CED for the treatment of tumors.

Since the infusions in this study were performed in formalin fixed brains, active transport across cellular membranes and blood perfusion were not a factor in the infusate distribution. The pilot pressure study showed the IPP was significantly lower as the temperature increased. We expected this would happen and would be a major factor in the increases in V_d with elevated temperatures. We also found that there was a large amount of intracellular Evan's blue after infusions at 42°C in formalin fixed tissue. This is suggestive of a significant increase in cell membrane permeability allowing the infusate to enter the cell. As mentioned previously, delivering a large amount of the therapeutic transcellular rather than paracellular, would limit the amount of drug metabolized after delivery and limit drug loss through tumor capillaries, which typically do not have an intact BBB. Since tumors often have an elevated IFP, transcellular delivery would also decrease the amount of efflux of the infusate from the interstitial spaces post infusion.

The histomorphological evaluation showed a large amount of pericellular vacuolization after CED infusion in the 22°C cortex. There is a small amount of pericellular clearing in

the untreated control cortex slide as well, which is an artifact of fixation and staining. The augmentation of this artifact in the 22°C cortex is likely related to the increased IPP. Infusing tissue with an elevated pressure causes the pressure to increase even more, this is likely why the 22°C cortex slide is so vacuolated. This increased pressure can lead to reflux and poor drug delivery. This artifact wasn't as obvious in the hippocampus and in the white matter, likely because it was farther from the FMD tip and did not experience the same pressure changes. Unfortunately we did not monitor the pressures of the infusion in real time to confirm this theory.

The Evan's blue was infused at room temperature, since we relied on the water bath to elevate the temperatures rather than laser light through the FMD. This would not have decreased the viscosity of the infusate prior to the infusion, which may be part of the reason the V_d/V_i ratios were smaller in this study compared to the in vivo rat study. This may have also cooled the brain tissue around the FMD tip, which may also account in part for the lower V_d/V_i ratios. The water bath was chosen over laser light to induce the hyperthermia in order to eliminate possible variations in the laser's ability to heat fixed tissue.

The room the infusions were performed in was approximately 24°C. The water bath unit was not able to keep the temperature of the water, therefore the brains, at a temperature lower than the room consistently accounting for the significant difference between actual and goal temperature for the 22°C group. The water bath unit was set between 12.2°C and 15°C, much lower than the goal of 22°C. On the other hand, the water bath had a

much easier time increasing the temperature with no significant difference between the actual and goal temperatures for the 37°C and 42°C groups.

Chapter 5: Conclusions

In conclusion, there may not have been a significant difference in V_d between all groups; however, the V_d did increase as the temperature was increased. The lack of significance is most likely secondary to the small sample size and the fact that one of the brains in the 37°C group was excluded. As the temperature is increased, the intraparenchymal pressure decreases making it easier for an infusate to travel through the tissue distributing itself within a larger volume. We also found at 42°C, there was a large amount of intracellular Evan's blue, indicating transcellular infusate distribution. This study in combination with the agarose phantom and in vivo rat studies show the potential for FMD technology to impact the way neurologic disease is treated in both people and companion animals. The next step for the FMD in regards to brain tumor treatment is a clinical trial with canine glioma patients.

Appendix A: Adult Mouse Brain Optical Clearance using Sca*l*e A2

When microscopically examining tissue, light is only able to penetrate a couple millimeters preventing visualization of the deeper structures. The reason for this is the heterogeneous nature of tissue, which is made up of cell membranes, cytoplasm, organelles, extracellular fluid and connecting tissue. All of these components have a different refractive index, causing scattering of light. Tissue optical clearance protocols are being developed to examine tissue in vivo and in vitro. These procedures cause tissue to become transparent to various degrees, by homogenizing the tissue's refractive index. There are different types of optical clearing protocols, however most rely on either dehydration or molecular changes between the tissue and the clearing agent, which is often reversible [62].

Tissue optical clearance has many uses in both the clinical and research setting. Clinically, clearing tissue in vivo can help determine blood flow, visualize vascular anomalies, aid in tattoo removal and many other applications. Further research is needed as to its safety in living tissue. There are many in vitro studies, especially in regards to the nervous system. Visualization of nervous tissue microscopically is limited to small tissue sections making it difficult to map neural connections. Optically clearing tissue can help researchers visualize the entire brain at one time, determining neuronal interconnections [62-64].

Sca*l*e is an optical clearing protocol that works differently than most other described tissue dehydration processes [62,64]. Sca*l*e results in tissue hydration via urea, and doubling the size of the tissue sample. This process requires fixed tissue samples, therefore is not applicable to in vivo studies. Sca*l*e A2 was shown to be effective in clearing whole mouse brains and embryos. It will also preserve florescence in labeled tissue [64]. Sca*l*e A2 is made up of 4M urea, 0.1% Triton X-100 and 10% glycerol. The solution can be stored at room temperature until ready for use. The following is the recommended protocol for clearing a mouse brain, which was used in the studies described below

1. Fix mouse brain with 4% paraformaldehyde
2. Post-fix the brain in 4% paraformaldehyde at 4°C for 8-12 hours
3. Wash the brain with phosphate buffered saline (PBS) then incubate in 20% sucrose solution at 4°C for 1-2 days
4. Embed the sample in optical cutting temperature (OCT) compound and freeze with liquid nitrogen
5. Thaw in PBS at room temperature for 20 minutes while agitating sample gently
6. Rise with PBS at room temperature for 20 minutes while agitating sample gently
7. Fix in 4% paraformaldehyde at room temperature for 30 minutes
8. Place the brain in Sca*l*e A2 solution while agitating gently until optically clear

The authors note that Mice older than 3 weeks may be more difficult and take longer to clear [64].

The Sca*l*e A2 solution with the above outlined protocol was originally used to attempt to clear a formalin fixed adult canine brain. The brain only became slightly transparent on the very superficial aspects after six months of incubation. I believe this is because the sample was too large, however given more time (years) it may clear more completely. This solution may work better on sections of canine brain to increase the surface area exposed to the clearing agent. This solution and protocol were also used to clear adult male Balb-c mouse brains (the same group of mice used for the CED infusions in the main body of this thesis). While this protocol did optically clear adult mouse brains, it took approximately 6 months until the brains were transparent, compared to 2 weeks reported to clear entire mouse embryos [64] (see figure A.1). As expected, the brains were much larger in size after clearing and the tissue was fragile. We have also used the technique to optically clear fluorescence vessel painted neonatal mouse brains (see figure A.2) for the laboratory of Dr. Michelle H. Theus. Visualization of the vessel painting was preserved in these samples following optical clearing.

Cleared brains could be used to both demonstrate and evaluate CED in the future. We originally embodied the use of the optically cleared brains for a visual experiment designed to simply but elegantly illustrate the principles and techniques of CED in real-time. We would expect the FMD with laser power to heat a larger volume of optically cleared brain tissue because the laser light could penetrate a larger volume of tissue. This may lead to a larger V_d in cleared brains. Further research with the Sca*l*e A2 solution will continue along with the laboratory of Dr. John Rossmeisl (Veterinary and Comparative Neuro-oncology laboratory).

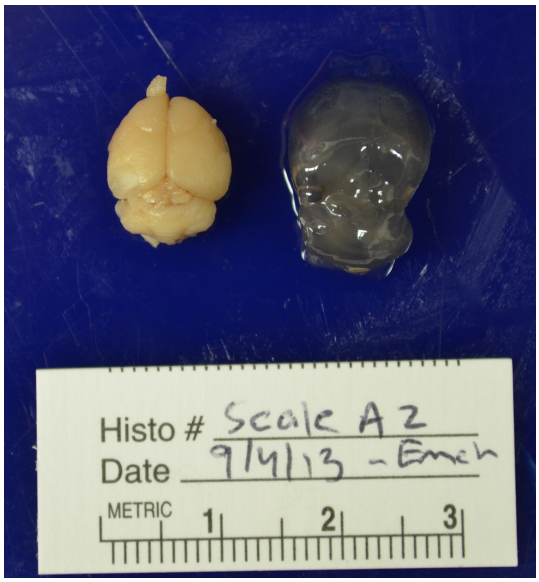

Figure A.1- Formalin fixed mouse brain (left) and optically clear mouse brain (right) after 6 months incubated in Sca*l*e A2 solution.

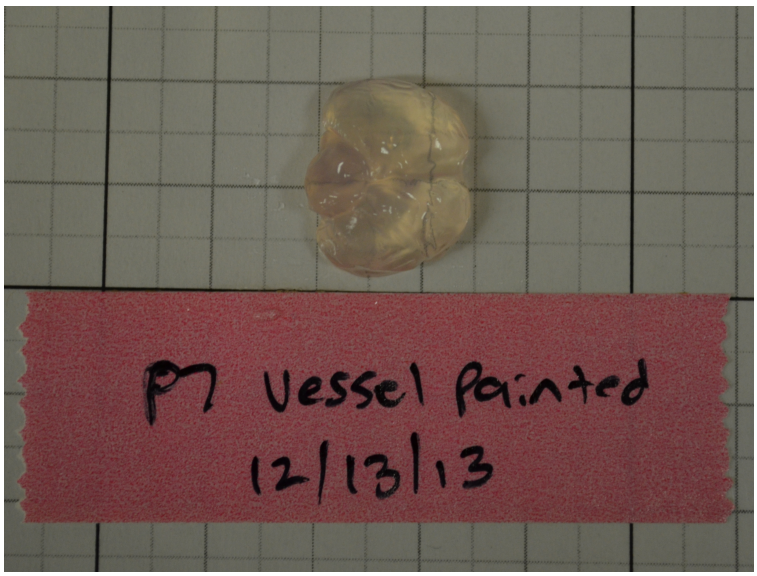

Figure A.2- Optically clear vessel painted brain 7 days postnatal. Photograph courtesy of the laboratory of Dr. Michelle H. Theus.

References

[1] Snyder JM, Shofer FS, VanWinkle TJ, Massicotte C. Canine intracranial primary neoplasia: 173 cases (1986-2003). J Vet Intern Med 2006;20:669-675.

[2] Dickinson PJ. Advances in Diagnostic and Treatment Modalities for Intracranial Tumors. J Vet Intern Med 2014; 28:1165–1185.

[3] Stoica G, Levine J, Wolff J, Murphy K. Canine astrocytic tumors: a comparative review. Vet Path 2011;48:266-275.

[4] Song R, Vite CH, Bradley CW, Cross JR. Postmortem evaluation of 435 cases of intracranial neoplasia in dogs and relationship of neoplasm with breed, age and body weight. J Vet Intern Med 2013; 27:1143–1152.

[5] Vandergrift WA, Patel SJ. Convection-enhanced delivery of immunotoxins and radioisotopes for treatment of malignant gliomas. Neurosurg Focus 2006;20:E13.

[6] White E, Bienemann A, Taylor H, Hopkins K, Cameron A, Gill S. A phase I trial of carboplatin administered by convection-enhanced delivery to patients with recurrent/progressive glioblastoma multiforme. Contemporary Clinical Trials 2012;33:320-331.

[7] Rock K, McArdle O, Forde P, Dunne M, Fitzpatrick D, O'Neill B, et al. A clinical review of treatment outcomes in glioblastoma multiforme – the validation in a non-trial population of the results of a randomized phase III clinical trial: has a more radical approach improved survival?. British Jounral of Radiology 2012;85:729-733.

[8] Thomas R, Duke SE, Wang HJ, Breen TE, Higgins RJ, Linder KE, et al. 'Putting our heads together': insights into genomic conservation between human and canine intracranial tumors. J Neurooncol 2009;94:333-349.

[9] Omuro A, DeAngelis LM. Glioblastoma and other malignant gliomas a clinical review. JAMA 2013;310:1842-1852.

[10] Kraft S, Gavin PR, DeHaan C, Moore M, Wendling LR, Leathers CW. Retrospective review of 50 canine intracranial tumors evaluated by magnetic resonance imaging. J Vet Intern Med 1997;11:218-225.

[11] Thomas WB, Wheeler SJ, Kramer R, Kornegay JN. Magnetic resonance imaging features of primary brain tumors in dogs. Vet Rad Ultrasound 1996;37:20-27.

[12] Young BD, Levine JM, Porter BF, Chen-Allen AV, Rossmeisl JH, Platt SR, et al. Magnetic resonance imaging features of intracranial astrocytomas and oligodendrogliomas in dogs. Vet Rad Ultrasound 2011;52:132-141.

[13] Louis DN, Ohgaki H, Wiestler OD, Cavenee WK, Burger PC, Jouvet A, et al. The 2007 WHO classification of tumors of the central nervous system. Acta Neuropathol 2007;114:97-109.

[14] Summers BA, Cummings JF, de Lahunta A. Veterinary Neuropathology. St Louis, Missouri: Mosby-Year Book, 1995.

[15] Kleihues P, Louis DN, Scheithauer BW, Rorke LB, Reifenberger G, Burger PC, et al. The WHO classification of Tumors of the Nervous System. J Neuropathology and Experimental Neurology 2002;61:215-225.

[16] Reitman ZJ, Olby NJ, Mariani CL, Thomas R, Breen M, Bigner DD, et al. IDH1 and IDH2 hotspot mutations are not found in canine glioma. International J Cancer 2010;127:245-247.

[17] Stoica G, Kim HT, Hall DG, Coates JR. Morphology, immunohistochemistry and genetic alterations in dog astrocytomas. Vet Pathol 2004;41:10-19.

[18] Rossmeisl JH, Jones JC, Zimmerman KL, Robertson JL. Survival time following hospital discharge in dogs with palliatively treated primary brain tumors. JAVMA 2013;242:193-198.

[19] Brearley MJ, Jeffery ND, Phillips SM, Dennis R. Hypofractionated radiation therapy of brain masses in dogs: a retrospective analysis of survival of 83 cases (1991-1996). J Vet Intern Med 1999;13:408-412.

[20] Haar CP, Hebbar P, Wallace GC, Das A, Vandergrift III WA, Smith JA, et al. Drug resistance in glioblastoma: a mini review. Neurochem Res 2012;37:1192-1200.

[21] Lai A, Tran A, Nghiemphu PL, Pope WB, Solis OE, Selch M, et al. Phase II study of bevacizumab plus temozolomide during and after radiation therapy for patients with newly diagnosed glioblastoma multiforme. J Clin Oncol 2011;29:142-148.

[22] Larson EW, Peterson HE, Lamoreaux WT, MacKay AR, Fairbanks RK, Call JA, et al. Case series: gamma knife as salvage therapy for recurrent glioblastoma multiforme. Brain disord Ther 2014;3:143.

[23] Pawlik TM, Keyomarsi K. Role of cell cycle in mediating sensitivity to radiotherapy. Int J Radiation Oncology Biol Phys 2004;59:928-942.

[24] Benczik J, Tenhunen M, Snellman M, Joensuu H, Farkkila M, Joensuu R, et al. Late radiation effects in the dog brain: correlation of MRI and histological changes. Radiotherapy and Oncology 2002;63:107-120.

[25] Bley CR, Sumova A, Roos M, Kaser-Hotz B. Irradiation of brain tumors in dogs with neurologic disease. J Vet Intern Med 2005;19:849-854.

[26] Garcia PA, Pancotto T, Rossmeisl JH, Henao-Guerrero N, Gustafson NR, Daniel GB, et al. Non-thermal irreversible electroporation (N-TIRE) and adjuvant fractionated radiotherapeutic multimodal therapy for intracranial malignant glioma in a canine patient. Technology in Cancer Research and Treatment 2011;10:73-83.

[27] Hawkins BT, Davis TP. The blood-brain barrier/neurovascular unit in health and disease. Pharmacol Rev 2005;57:173-185.

[28] Deeken JF, Loscher W. The blood-brain barrier and cancer: transporters, treatment and the Trojan horses. Clin Cancer Res 2007;13:1663-1674.

[29] Abbott NJ, Romero IA. Transporting therapeutics across the blood-brain barrier. Molecular Med Today 1996;96:1357-4310.

[30] Pardridge WM. Blood-brain barrier delivery. Drug Discovery Today 2007;12:54-61.

[31] Bentivoglio M, Kristensson K. Tryps and trips: cell trafficking across the 100-year-old blood-brain barrier. Trends in Neurosciences 2014;37:325-333.

[32] Liu HL, Hua MY, Chen PY, Chu PC, Pan CH, Yang HW, et al. Blood-brain barrier disruption with focused ultrasound enhances delivery of chemotherapeutic drugs for glioblastoma treatment. Radiology 2010;255:415-425.

[33] White E, Bienemann A, Taylor H, Hopkins K, Cameron A, Gill S. A phase I trial of carboplatin administered by convection-enhanced delivery to patients with recurrent/progressive glioblastoma multiforme. Contemporary Clinical Trials 2012;33:320-331.

[34] Kanner AA. Convection-enhanced delivery. In: Barnett GH eds. Current Clinical Oncology: High-Grade Gliomas: Diagnosis and Treatment. Totowa,NJ: Humana Press, 2010, pp. 303-314.

[35] Ding D, Kanaly CW, Brady ML, Mittermeyer S, Raghavan R, Sampson JH. Convection-Enhanced drug delivery to the brain. In: Jain KK eds. Drug Delivery to the CNS. New York: Humana Press, 2010, pp. 291-313.

[36] Raghavan R, Brady ML, Rodriguez-Ponce MI, Hartlep A, Pedain C, Sampson JH. Convection-enhanced delivery of therapeutics for brain disease, and its optimization. Neurosurg Focus 2006;20:E12.

[37] Dickinson PJ, LeCouteur RA, Higgins RJ, Bringas JR, Larson RF, Yamashita Y, et al. Canine spontaneous glioma: a translation model system for convection-enhanced delivery. Neuro-Oncology 2010;12:928-940.

[38] Platt S, Ndumon E, Kent M, Freeman C, Machaidze R, Kaluzova M, et al. Canine model of convection-enhanced delivery of cetuximab conjugated iron-oxide nanoparticles monitored with magnetic resonance imaging. Clin Neurosurg 2012;59:107-113.

[39] Sampson JH, Archer G, Pedain C, Wembacher-Schroder E, Westphal M, Kunwar S, et al. Poor drug distribution as a possible explanation for the results of the PRECISE trial. J Neurosurg 2010;113:301-309.

[40] Bobo RH, Laske DW, Akbasak A, Morrison PF, Dedrick RL, Oldfield EH. Convection-enhanced delivery of macromolecules in the brain. Proc Natl Acad Sci 1994;91:2076-2080.

[41] Vazquez LC, Hagel E, Willenberg BJ, Dai W, Casanova F, Batich CD, et al. Polymer-coated cannulas for the reduction of backflow during intraparenchymal infusions. J Mater Sci: Mater Med 2012; 23:2037-2046.

[42] Leunig M, Goetz AE, Dellian M, Zetterer G, Gamarra F, Jain RK, et al. Interstitial fluid pressure in solid tumors following hyperthermia: possible correlation with therapeutic response. Cancer Research 1992;52:487-490.

[43] Hood RL, Andriani RT, Emch S, Robertson JL, Rylander CG, Rossmeisl JH. Fiberoptic microneedle device facilitates volumetric infusate dispersion during convection-enhanced delivery in the brain. Lasers in Surgery and Medicine 2013;45:418-426.

[44] Bischof JC, Padanilam J, Holmes WH, Ezzell RM, Lee RC, Tompkins RG, et al. Dynamics of cell membrane permeability changes at supraphsiological temperatures. Biophysical Journal 1995;68:2608-2614.

[45] Elmoazzen HY, Elliott JAW, McGann LE. The effect of temperature on membrane hydraulic conductivity. Cryobiology 2002;45:68-79.

[46] Falk MH, Issels RD. Hyperthermia in oncology. Int J Hyperthermia 2001;17:1-18.

[47] Vogi TJ, Farshid P, Naguib NNN, Zangos S. Thermal ablation therapies in patients with breast cancer liver metastases: a review. Eur Radiol 2013;23:797-804.

[48] Silberman AW, Morgan DF, Storm FK, Rand RW, Benz M, Drury B, et al. Combination radiofrequency hyperthermia and chemotherapy (BCNU) for brain malignancy. J of Neuro-Oncology 1984;2:19-28.

[49] Uzuka T, Takahashi H, Tanaka R. Interstitial hyperthermia with intra-arterial injection of Adriamycin for malignant glioma. Neurol Med Chir 2006;46:19-23.

[50] Muralidharan V, Christophi C. Interstitial laser thermotherapy in the treatment of colorectal liver metastases. J Surg Oncol 2001;76:73-81.

[51] Menovsky T, Beek JF, van Gemert MJC, Roux FX, Brown SG. Interstitial laser thermotherapy in neurosurgery: a review. Acta Neurochir 1996;138:1019-1026.

[52] Kosoglu MA, Hood RL, Rossmeisl JH, Grant DC, Xu Y, Robertson JL, et al. Fiberoptic microneedles: novel optical diffusers for interstitial delivery of therapeutic light. Lasers in Surg Med 2011;43:914-920.

[53] Hood RL, Ecker T, Andriani R, Robertson J, Rossmeisl J, Rylander CG. Augmenting convection-enhanced delivery through simultaneous co-delivery of fluids and laser energy with a fiberoptic microneedle device. Optical Fibers and Sensors for Medical Diagnostics and Treatment Applications XIII 2013;8576:85760G.

[54] Yaroslavsky AN, Schulze PC, Yaroslavsky IV, Schober R, Ulrich F, Schwarzmainer HJ. Optical properties of selected native and coagulated human brain tissues in vitro in the visible and near infared spectral range. Phys Med Biol 2002;47:2059-2073.

[55] Hood RL, Rossmeisl JH, Andriani RT, Wilkinson AR, Robertson JL, Rylander CG. Intracranial hyperthermia through local photothermal heating with a fiberoptic microneedle device. Lasers in Surg Med 2013;45:167-174.

[56] Andriani RT. Design and Validation of Medical Devices for Photothermally Augmented Treatments. 2014; Blacksburg, VA. Master's Thesis.

[57] Paxinos G, Franklin KBJ. The Mouse Brain in Stereotaxic Coordinates. San Diego: Elsevier Science, 2004.

[58] Los G, Sminia P, Wondergem J, Mutsaers PHA, Havemen J, Huinink DB, et al. Optimisation of intraperitoneal cisplatin therapy with regional hypterthemia in rats. Eur J Cancer 1991;27:472-477.

[59] Mayhew TM, Olsen DR. Magnetic resonance imaging (MRI) and model-free estimates of brain volume determined using the Cavalieri principle. J Anat 1991;178:133-144.

[60] Kiernan JA. Formaldehyde, formalin, paraformaldehyde and glutaraldehyde: what they are and what they do. Microscopy Today 2000;00-1:8-12.

[61] Boucher Y, Salehi H, Witwer B, Harsh GR, Jain RK. Interstitial fluid pressure in intracranial tumors in patients and in rodents. British Journal of Cancer 1997;75:829-836.

[62] Zhu D, Larin KV, Luo Q, Tuchin VV. Recent progress in tissue optical clearing. Laser Photonics Rev 2013;5:732-757.

[63] Shen H. See-through brains clarify connections. Nature 2013;496:151.

[64] Hama H, Kurokawa H, Kawano H, Ando R, Shimogori T, Noda H. Sca*l*e: a chemical approach for fluorescence imaging and reconstruction of transparent mouse brain. Nature Neuroscience 2011;14:1481-1488.